Article

Theoretical Study of the Effects of Different Coordination Atoms (O/S/N) on Crystal Structure, Stability, and Protein/DNA Binding of Ni(II) Complexes with Pyridoxal-Semi, Thiosemi, and Isothiosemicarbazone Ligand Systems

Violeta Jevtovic [1,†], Aleksandra Rakić [2,†], Odeh A. O. Alshammari [1], Munirah Sulaiman Alhar [1], Tahani Alenezi [1], Violeta Rakic [3] and Dušan Dimić [2,*]

[1] Department of Chemistry, College of Science, University of Ha'il, Ha'il 81451, Saudi Arabia
[2] Faculty of Physical Chemistry, University of Belgrade, Studentski trg 12–16, 11000 Belgrade, Serbia
[3] Department of Agriculture and Food Technology Studies Prokuplje, Toplica Academy of Applied Studies, Ćirila i Metodija 1, 18400 Prokuplje, Serbia
* Correspondence: ddimic@ffh.bg.ac.rs
† These authors contributed equally to this work.

Abstract: Nickel transition metal complexes have shown various biological activities that depend on the ligands and geometry. In this contribution, six Ni(II) nitrate complexes with pyridoxal-semi, thiosemi, and isothiosemicarbazone ligands were examined using theoretical chemistry methods. The structures of three previously reported complexes ([Ni(PLSC)(H$_2$O)$_3$]·2NO$_3^-$, [Ni(PLTSC)$_2$]·2NO$_3^-$·H$_2$O, and [Ni(PLITSC)(H$_2$O)$_3$]·2NO$_3^-$) were investigated based on Hirshfeld surface analysis, and the most important stabilization interactions in the crystal structures were outlined. These structures were optimized at the B3LYP/6-311++G(d,p)(H,C,N,O,(S))/LanL2DZ(Ni) level of theory, and the applicability was checked by comparing theoretical and experimental bond lengths and angles. The same level of theory was applied for the optimization of three additional structures, ([Ni(PLSC)$_2$]$^{2+}$, [Ni(PLTSC)(H$_2$O)$_3$]$^{2+}$, and [Ni(PLITSC)$_2$]$^{2+}$). The interactions between selected ligands and Ni(II) were examined using the Natural Bond Orbital (NBO) and Quantum Theory of Atoms in Molecules (QTAIM) approaches. Particular emphasis was placed on interactions between oxygen, sulfur, and nitrogen donor atoms and Ni(II). Human Serum Albumin (HSA) and the DNA-binding properties of these complex cations were assessed using molecular docking simulations. The presence of water molecules and various substituents in the thermodynamics of the processes was demonstrated. The results showed significant effects of structural parameters on the stability and reactivity towards important biomolecules.

Keywords: nickel(II) complexes; DFT; QTAIM; HSA; DNA; molecular docking

1. Introduction

Transition metal complexes are an important group of compounds with pronounced biological activity. They are commonly used in medicine as contrast agents in Magnetic Resonance Imaging (MRI), radiopharmaceuticals, chemotherapeutics, and compounds for arthritis treatment [1]. The success of platinum compounds in suppressing cell division led to the introduction of transition metal complexes in modern medical research. The primary mechanism of cisplatin action includes binding to DNA molecules and disrupting the transcription process [2,3]. The limited selectivity and toxicity of cisplatin and the development of resistance led to research on other transition metal complexes. Platinum and ruthenium ions and their compounds have been the most widely investigated [4]. However, cheaper first-row transition metals are being examined as potential alternatives for efficient cytotoxic agents [5]. Nickel is one of the essential elements in biological systems, and it constitutes several metalloproteins.

Nickel complexes are being investigated as antibacterial, leishmanicidal, antifungal, anticancer, antioxidant, and antiretroviral agents [6–10]. The nature of coordinating ligands influences these compounds' thermodynamic and kinetic stability [1]. It has been shown that the size and shape of octahedral nickel complexes directly affect DNA affinity [11].

Complexes containing semi- and thiosemicarbazone ligands have attracted the attention of scientists due to their interesting structural characteristics and the possibility of complexation to different transition metals [12]. The biological activity of these compounds includes potential use as radioprotectors, anti-protozoa agents, chelating ligands, and antimicrobials [13]. The thiosemicarbazone complexes have shown a broader spectrum of biological activities, as discussed in [14]. Thiosemicarbazones ($R^1R^2C^2=N^3-N^2(H)-C^1(=S)N^1R^3R^4$) are a diverse group of ligands containing both nitrogen and sulfur donor atoms. They are prepared via condensation between ketone or aldehyde and thiosemicarbazide. Depending on protonation, these ligands form differently charged complexes [15]. Pyridoxal–thiosemicarbazone (PLTSC) is formed by reacting pyrodixal, a vitamin B6 analog, and thiosemicarbazone [12]. A comprehensive review of the transition metal complexes with PLTSC is presented in [13]. The pyridoxal–semicarazone (PLSC) ligand is an oxygen analog of PLTSC, with ONO donor atoms [12]. The third ligand of interest for this study is pyridoxal-S-methylisothiosemicarbazone (PLITSC), formed in the reaction between pyridoxal and S-methyl-isothiosemicarbazone. In this ligand, the sulfur atom is protected by the presence of a methyl substituent, which leads to an ONN donor system. PLITSC can also be found in neutral, mono, and dianionic forms [16]. The structures of neutral PLSC, PLTSC, and PLITSC ligands are presented in Figure 1.
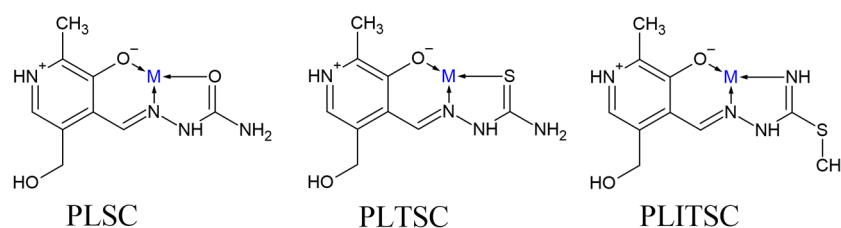

Figure 1. Complexation modes of neutral PLSC, PLTSC, and PLITSC ligands.

Several Ni(II) complexes containing the mentioned ligands have been described in the literature. Jevtović et al. investigated the effects of metal ions (Fe, Co, Ni, and Cu) in complexes with PLTSC ligands on structural properties, protein binding, and cytotoxicity [17]. The crystal structure of [Ni(PLTSC)$_2$]·2NO$_3^-$·H$_2$O was similar to the previously obtained one by Leovac et al. [12]. Density functional theory (DFT) optimization of structure at the B3LYP/6-311++G(d,p)(H,C,N,O,(S))/LanL2DZ(Ni) level of theory gave bond lengths and angles comparable to the experimental ones, and this structure was used for further theoretical analyses. The experimental transport protein binding affinity of the mentioned complex was further verified by molecular docking. Synthesis, X-ray structures, and spectra of two complexes containing PLSC and PLITSC neutral ligands along with three molecules of water ([Ni(PLSC)(H$_2$O)$_3$]·2NO$_3^-$ and [Ni(PLITSC)(H$_2$O)$_3$]·2NO$_3^-$·H$_2$O) were described in references [18,19]. Other Ni(II) complexes with three ligands from Figure 1 include [Ni(PLSC-H)2]·H$_2$O [20], [Ni(PLSC)Cl$_2$]·3.5H$_2$O, [Ni(PLSC)(NCS)$_2$]·4H$_2$O, [Ni(PLSC-2H)NH$_3$]·1.5H$_2$O, [Ni(PLTSC-H)NCS], [Ni(PLTSC-H)py]·2NO$_3^-$ (py-piridine) [18], [Ni(PLTSC-H)(NO$_3$)]·2H$_2$O, and [Ni(PLTSC-2H]·2H$_2$O [21], and their structural and spectral properties are described in a review paper by Leovac et al. [13]. Structures with other counterions are also known [22].

This paper aims to investigate the differences in the crystal structure, stability, and protein/DNA affinity of Ni(II) nitrate complexes with PLSC, PLTSC, and PLITSC ligands. The crystal structures of known complexes, namely [Ni(PLSC)(H$_2$O)$_3$]·2NO$_3^-$, [Ni(PLTSC)$_2$]·2NO$_3^-$, and [Ni(PLITSC)(H$_2$O)$_3$]·2NO$_3^-$, were examined using Hirshfeld surface analysis, and the percentages of different stabilization interactions were compared. The structures of complex cations from these crystal structures, together with three theoretical cations ([Ni(PLSC)$_2$]$^{2+}$, [Ni(PLTSC)(H$_2$O)$_3$]$^{2+}$, and [Ni(PLITSC)$_2$]$^{2+}$), were optimized at the B3LYP/6-311++G(d,p)(H,C,N,O,(S))/LanL2DZ(Ni) level of theory. The changes in bond lengths and overall geometry were discussed based on the

present donor atoms. The Quantum Theory of Atoms in Molecules (QTAIM) was applied to examine the strength of coordination bonds between various donor atoms and nickel(II). The molecular docking study was used to determine the affinity of these complex cations towards Human Serum Albumin (HSA), a significant transport protein, and DNA. The effects of ligand structure and the presence of water molecules on the interaction with biomolecules were outlined.

2. Results and Discussion

2.1. Hirshfeld Surface Analysis

Selected crystal structures of nickel(II) nitrate complexes with PLSC, PLTSC, and PLITSC were examined using Hirshfeld surface analysis. These three structures were chosen because all contain nickel in +2 state, a ligand in a neutral form, a charge of the complex cation of +2, and surrounding nitrate counterions. Therefore, these structures allow for the elucidation of the most important contacts in the crystal structures, as three ligands differ in the donor atoms attached to central metal ion. Figure 2 presents the Hirshfeld surfaces of these complex compounds, while the most important contacts are listed in Table 1. The fingerprint plots of the most numerous contacts are given in Figures S1–S3. It is important to outline that only the complex cation was included when examining the stabilization interactions, as the positions of nitrate counterions are significantly different in the examined structures.
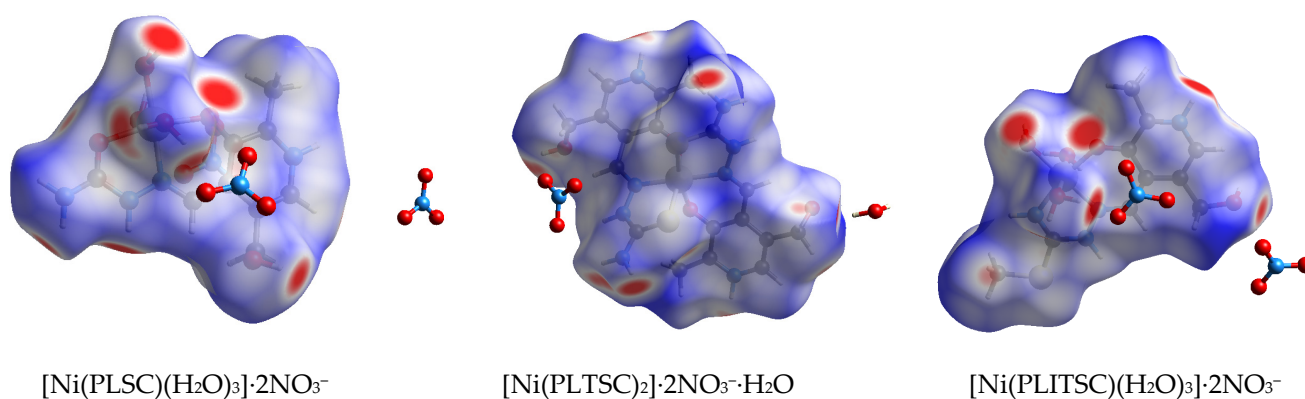

$[Ni(PLSC)(H_2O)_3] \cdot 2NO_3^-$ $[Ni(PLTSC)_2] \cdot 2NO_3^- \cdot H_2O$ $[Ni(PLITSC)(H_2O)_3] \cdot 2NO_3^-$

Figure 2. Hirshfeld surfaces of different nickel(II) nitrate complexes included in this study.

Table 1. Percentages of the most important contacts in the crystallographic structures determined based on Hirshfeld surface analysis.

Contact	$[Ni(PLSC)(H_2O)_3] \cdot 2NO_3^-$	$[Ni(PLTSC)_2] \cdot 2NO_3^- \cdot H_2O$	$[Ni(PLITSC)(H_2O)_3] \cdot 2NO_3^-$
O···H	49.7	36.3	43.8
H···H	31.5	27.4	36.1
N···H	3.4	4.7	2.4
C···H	5.5	9.7	3.9
O···N	1.9	1.8	0.5
O···O	1.7	0.6	/
O···C	4.1	1.3	4.0
N···C	1.4	0.5	/
S···H	/	10.4	2.2
S···C	/	2.8	2.0
S···O	/	0.3	1.8
S···N	/	0.9	1.0

The octahedral geometry of three complexes excludes the possibility of interactions involving the central metal ion, as previously discussed for similar compounds [17,23]. The most numerous contacts include oxygen and hydrogen atoms. The percentages of O···H contacts are 49.1, 36.3, and 43.8% for the three complexes (Table 1). This value is higher when water molecules are present. The highest percentage in the case of $[Ni(PLSC)(H_2O)_3] \cdot 2NO_3^-$ is expected, since PLSC contains one oxygen atom more than the PLITSC ligand. The red spots on the Hirshfeld surfaces denote the positions of hydrogen

bonds, where most are located around water molecules. These complexes act mainly as hydrogen atom donors through water molecules and the OH group attached to the pyridine ring. In the crystal structure of the Ni(II) complex with a deprotonated PLSC ligand, the amount of O···H interactions is 23.3% due to the decrease in the number of hydrogen bonds [20]. The second-most numerous contacts are formed between hydrogen atoms, ranging from 27.4 to 36.1%. These interactions are usually weaker and include interactions between hydrogen atoms attached to different atoms. The relative abundance of hydrogen atoms in ring structures, water molecules, and methyl group of PLITSC is responsible for forming these interactions. Strong hydrogen bonds also include N···H contacts. The protonated nitrogen atoms of the pyridine ring, aliphatic chain, and ending amino group of PLSC and PLTSC ligands are suitable for the formation of stabilization interactions. The percentage of N···H (2.4%) is the lowest in the third complex due to the exchange of amino group with –S(CH$_3$). The interactions between carbon and hydrogen atoms, denoted as C···H, have percentages between 3.9 and 9.7%, consistent with previously investigated dioxovanadium(V) complexes with PLSC, PLTSC, and PLITSC ligands [24]. The existence of two ligand molecules in the second complex increases the amount of carbon atoms and the abundance of the interactions. Again, the presence of methyl group in PLITSC, compared to PLSC, leads to an increase in the amount of C···H contacts. The interactions between positively charged hydrogen atoms and negatively charged π-electron clouds are also part of this group [25]. The position of the sulfur atom in the structure of PLTSC and PLITSC significantly influences the percentage of weaker hydrogen bonds (S···H). The methyl group attached to the sulfur atom limits the interactions, leading to a much lower percentage of 2.2% (Table 1).

Interactions between electronegative atoms also depend on the present substituents and relative positions of groups. In the first structure, the most numerous are N···O (1.9%) contacts due to the present groups. Once the oxygen atom is exchanged with sulfur, these interactions are lowered to 1.8% in the second structure. The O···O interactions are present only in the first two structures, proving that there is no direct contact between the water molecules of the two complex cations in the third structure. The abundance of oxygen atoms in the first structure is responsible for the formation of O···C interactions. Structures with sulfur also have a higher percentage of S···C interactions when compared to interactions with nitrogen and oxygen atoms. The effects of geometry and stabilization interactions will be investigated in the following structures.

2.2. DFT Optimization of Structures

The structures of three experimental and three theoretical structures were optimized at the B3LYP/6-311++G(d,p)(H,C,N,O,(S))/LanL2DZ(Ni) level of theory, as shown in Figure 3. The triplet state of the complexes was considered, as it was shown to be more stable than the singlet one [26]. The applicability of the selected level of theory was examined by comparing the crystallographic and optimized bond lengths and angles for ([Ni(PLSC)(H$_2$O)$_3$]$^{2+}$, [Ni(PLITSC)(H$_2$O)$_3$]$^{2+}$, and [Ni(PLTSC)$_2$]$^{2+}$ complex cations. These structures were extracted from previously discussed crystal structures. The quantitative parameters used for comparison were the correlation coefficient and mean absolute error (MAE). The second parameter calculates the average absolute difference between the two datasets. The experimental and theoretical structural parameters are listed in Tables S1–S3, while the R and MAE values are presented in Table 2. The optimization of theoretical structures was needed to further analyze the coordination of ligands to the central metal ions, as well as for the molecular docking simulations of the binding to transport proteins and DNA.

The optimized bond lengths coincide well with the crystallographic ones. The correlation coefficients are 0.96 for [Ni(PLITSC)(H$_2$O)$_3$]$^{2+}$ and 0.99 for the other two structures, with MAE values between 0.017 ([Ni(PLSC)(H$_2$O)$_3$]$^{2+}$) and 0.041 Å ([Ni(PLTSC)$_2$]$^{2+}$). These values were of the order of experimental error. In the first structure, the bond lengths between nickel(II) and water oxygen atoms are between 2.054 and 2.115 Å in the experimental structures and between 2.086 and 2.153 Å in the optimized structures. The distances between the central metal ion and

carbonyl group attached to the pyridine ring are 1.983 and 1.992 Å in the crystallographic and optimized structures, respectively. A larger distance is found between the second carbonyl group and Ni(II) (2.068/2.073 Å), while the Ni–N bond lengths are 2.016 (exp.) and 2.064 Å (theor.). A similar range of bond lengths between the central metal ion and coordinated water is found in the structure of $[Ni(PLITSC)(H_2O)_3]^{2+}$, between 2.041 and 2.131 Å, which proves the assumption that these bonds are not significantly influenced by the ligand structure. The change in the ligand structure of PLITSC in comparison to PLSC leads to lower bond distances between Ni(II) and the carbonyl group oxygen atom (1.880/1.999 Å) and the nitrogen atom of the azomethine group (1.938/2.078 Å). It is evident that due to the optimization and relaxation of the structure, the bond lengths in $[Ni(PLITSC)(H_2O)_3]^{2+}$ increase and become similar to the first complex. The distances between Ni(II) and the nitrogen donor atoms are 1.938 and 2.078 Å in the experimental and theoretical structures, which are comparable to when an oxygen atom is present. In the experimental structure of $[Ni(PLTSC)_2]^{2+}$, the bond lengths between the oxygen/nitrogen atoms and the central metal ion are 1.906/1.907 Å, which are lower than values found in the two complexes with coordinated water molecules. The bond distance between Ni(II) and sulfur is 2.277 in the experimental structure and 2.483 Å in the theoretical structure. Based on these values, it can be assumed that the weakest interactions include the sulfur atoms due to their low electronegativity and electron-donation ability. These assumptions are examined in detail in the following section. The bond lengths of atoms within PLSC, PLTSC, and PLITSC are within the expected range, as explained in references [16,24]. The extended delocalization within the ligand structures prevents significant changes in bond lengths upon complexation [17].
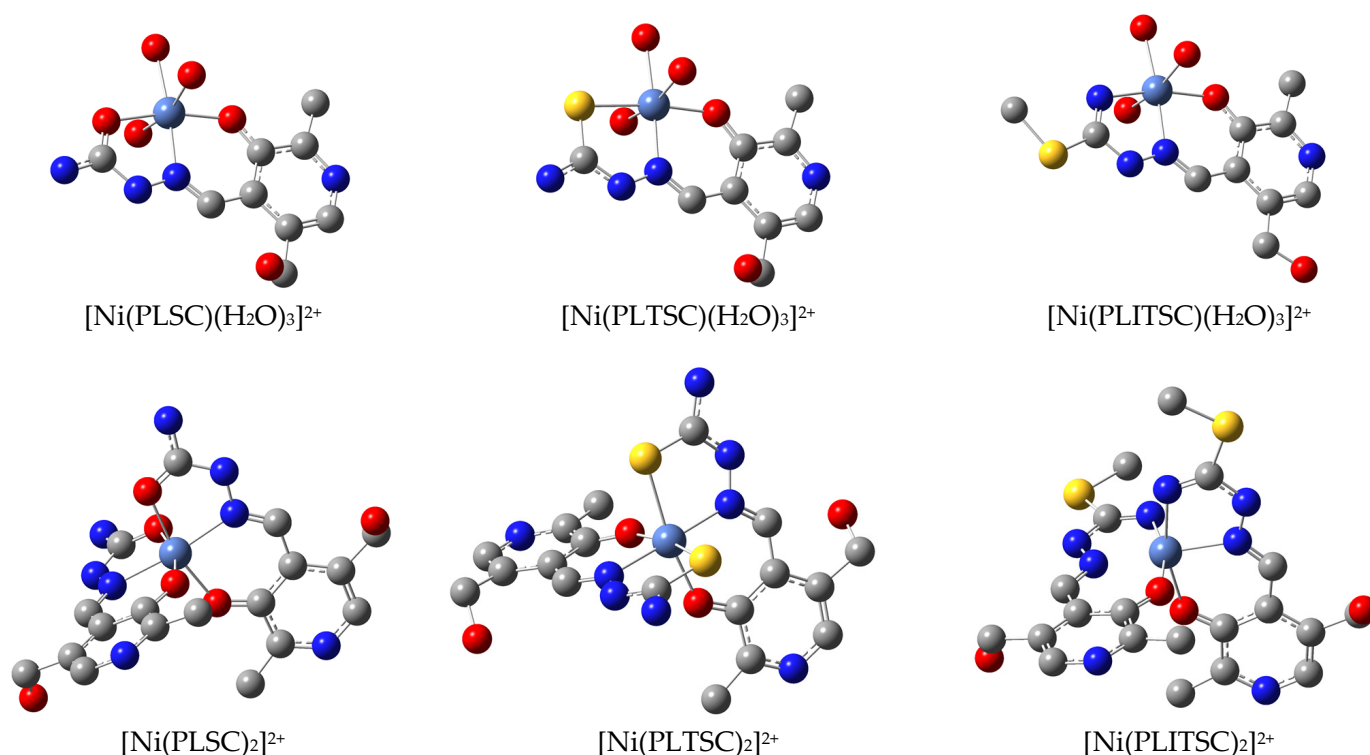

$[Ni(PLSC)(H_2O)_3]^{2+}$ $[Ni(PLTSC)(H_2O)_3]^{2+}$ $[Ni(PLITSC)(H_2O)_3]^{2+}$

$[Ni(PLSC)_2]^{2+}$ $[Ni(PLTSC)_2]^{2+}$ $[Ni(PLITSC)_2]^{2+}$

Figure 3. Optimized structures (at the B3LYP/6-311++G(d,p)(H,C,N,O,(S)/LanL2DZ(Ni) level of theory) of selected octahedral Ni(II) complexes. Carbon—gray; nitrogen—blue; oxygen—red; sulfur—yellow; nickel—teal; hydrogen atoms have been omitted for clarity.

Table 2. Bonding energy (BE), electron configuration of Ni, and charges on selected atoms in the optimized structures of complex cations at the B3LYP/6-311++G(d,p)(H,C,N,O,(S)/LanL2DZ(Ni) level of theory.

Complex Cation	BE [kJ mol^{-1}]	Electron Configuration Ni	Charge Ni	Charge O$_{arom}$	Charge N$_{azomethine}$	Charge X	Charge O$_{water}$
[Ni(PLSC)(H$_2$O)$_3$]$^{2+}$	−981	4s$^{0.23}$ 3d$^{8.27}$ 4p$^{0.40}$	1.096	−0.710	−0.300	−0.668 (O)	−0.906/−0.891/−0.906
[Ni(PLTSC)(H$_2$O)$_3$]$^{2+}$	−854	4s$^{0.27}$ 3d$^{8.32}$ 4p$^{0.51}$	0.899	−0.697	−0.287	−0.053 (S)	−0.900/−0.890/−0.900
[Ni(PLITSC)(H$_2$O)$_3$]$^{2+}$	−850	4s$^{0.24}$ 3d$^{8.28}$ 4p$^{0.43}$	1.045	−0.718	−0.285	−0.794 (N)	−0.889/−0.898/−0.898
[Ni(PLSC)$_2$]$^{2+}$	−2122	4s$^{0.26}$ 3d$^{8.29}$ 4p$^{0.44}$	1.003	−0.676/−0.675	−0.280/−0.279	−0.637/−0.637 (O)	/
[Ni(PLTSC)$_2$]$^{2+}$	−2082	4s$^{0.33}$ 3d$^{8.39}$ 4p$^{0.64}$	0.639	−0.656/0.654	−0.264/−0.261	−0.024/−0.024 (S)	/
[Ni(PLITSC)$_2$]$^{2+}$	−2150	4s$^{0.28}$ 3d$^{8.31}$ 4p$^{0.49}$	0.916	−0.667/−0.667	−0.267/−0.267	−0.736/−0.736 (N)	/

The bond angles are more prone to change upon optimization due to the system's relaxation, which leads to octahedral geometry. Nevertheless, the correlation coefficients are 0.99 for all three structures, with MAE values between 1.50 ([Ni(PLITSC)(H$_2$O)$_3$]$^{2+}$) and 1.94° ([Ni(PLTSC)$_2$]$^{2+}$). The optimization of the first crystal structure led to significant changes in bond angles that include water molecules. For example, the experimental value of the O2-Ni1-O3 is 86.94°, while the theoretical value is 82.30°. These changes of several degrees can be explained by the system's relaxation and the absence of interactions with surrounding units. The optimization was performed for isolated complexes in a vacuum, and certain differences were expected. The discrepancies between the two sets of data are less pronounced for angles including two donor atoms of the PLSC ligand, such as between the carbonyl group oxygen attached to the pyridine ring, Ni(II), and the nitrogen atom (89.69 (exp.) and 87.98° (theor.), Table S2). Again, the rigidity of the ligand prevents significant changes in the angle values. A similar result was found for the structure of the second examined complex cation, [Ni(PLITSC)(H$_2$O)$_3$]$^{2+}$. The third experimentally obtained complex contains two PLTSC ligands with three different donor atoms. The optimized structure is characterized by the change in angles; for example, the S–Ni–O angles, in which S and O belong to the same ligand, are equilibrated to 169°, although their experimental values were 179.29 and 164.36°. The increase in local symmetry is a consequence of the system's relaxation. The changes in the other angles are less pronounced, usually less than two degrees. It is important to mention that the crystal structure of [Ni(PLTSC)$_2$]·2NO$_3$$^-$·H$_2$O contains two counterions and a solvent molecule that influence the overall geometry through intermolecular interactions. Based on these results, it can be concluded that the selected level of theory optimized the structure of the examined complex cations well, and it could be applied to the structural examination of other theoretical structures and stabilization interactions.

The theoretical structures of the other three complex cations were optimized at the same level of theory. In the optimized structure of [Ni(PLTSC)(H$_2$O)$_3$]$^{2+}$, the bond length of Ni–S is 2.419 Å, which is higher than other bonds in corresponding complexes with PLSC and PLITSC ligands. A certain elongation of Ni–O bonds (carbonyl groups attached to aromatic ring/aliphatic chain, 2.123/2.028 Å) is also found in [Ni(PLSC)$_2$]$^{2+}$ compared to the structure with three molecules of water (2.073/1.992 Å). The presence of another ligand changes the positional preferences due to its size. The same can be observed in the structure of [Ni(PLITSC)$_2$]$^{2+}$, especially for the Ni–O (amino substituent). Therefore, these interactions were subjected to the QTAIM analysis to determine their type and strength.

The binding energy of ligands to the central metal ion was estimated using the following equations for mono and bisligand systems for the optimizations in the gas phase [27]:

$$\text{BE} = E(\text{monoligand complex}) - [(E(\text{Ni(H}_2\text{O)}_3)^{2+} - E(\text{ligand})] \tag{1}$$

$$\text{BE} = E(\text{bisligand complex}) - [(E(\text{Ni})^{2+} - 2E(\text{ligand})] \tag{2}$$

As explained in the Methodology section, the obtained values were corrected for the basis set superposition error. The binding energies, calculated at the B3LYP/6-311++G(d,p) (H,C,N,O,(S)/LanL2DZ(Ni) level of theory, are shown in Table 2, and they confirm the sta-

bility of the examined species. Caramori et al. discussed that several parameters influence the binding energy, such as the ligand size, hydrogen bonds, and electrostatic interactions between positively charged central metal ion and negatively charged ligands [28]. The highest binding energy for complex cations with three water molecules is calculated for the PLSC ligand (941 kJ mol^{-1}) due to an electronegative oxygen atom attached to an aliphatic chain. When a sulfur atom is present in the structure, the binding energies are lowered to 854 and 850 kJ mol^{-1}. These values are comparable to those found for Ni(II) complexes with chalcone-based Schiff bases [29]. Complex cations with two ligands show even higher binding energies of −2112 (PLSC), −2082 (PLTSC), and −2150 kJ mol^{-1} (PLITSC). It is important to observe that these energies are more than two times higher than the previously discussed ones, which leads to the conclusion that interactions with PLSC/PLTSC/PLITSC are stronger than those with three water molecules. The presence of four nitrogen atoms in the structure of [Ni(PLITSC)$_2$]$^{2+}$ and their electron-donating ability are the most important parameters for structure stability.

The natural atomic charges of nickel, oxygen, nitrogen, and sulfur atoms that form the coordination sphere are listed in Table 2, together with the electron configurations of Ni ions. The NBO analysis is an appropriate method for studying the charge transfer in compounds [30]. The electron configuration of the free metal ion is 4s^0 3d^8. The investigated complexes have an equal donation from each ligand to d and s orbitals, as the occupations are between 0.23 and 0.33 for the 4s orbital and 8.27 and 8.39 for the 3d orbital. A significant donation is observed for the 4p orbital (0.40–0.64). A much lower donation was found in square-planar Ni(II) complexes with Schiff bases synthesized from 2-hydroxy-5-methylbenzaldehyde, although nitrogen and oxygen atoms were also involved [31]. The octahedral Ni(II) complex with phenylacetic acid and 1,10′-phenanthroline contained significant donations to the 4p orbital [32]. The charges on Ni, O$_{arom}$, N$_{azomethine}$, and O$_{aliph}$ are 1.096, −0.710, −0.300, and −0.668 e, respectively. The expected values are 2, −2, −1, and −2 e, which proves the assumption that electron donation occurs from oxygen and nitrogen atoms' orbitals to the orbitals of the central metal ion. The charge on the water oxygen atoms is higher than on oxygen atoms attached to the pyridine ring and aliphatic chain. Interestingly, the electron donation of a water molecule in the same plane as the PLSC ligand is much higher than that of two other molecules. A lower charge on the nickel ion is calculated for [Ni(PLTSC)(H$_2$O)$_3$]$^{2+}$ due to the significant donation from the sulfur atom, especially to the 4p orbital. Once the sulfur atom is exchanged with nitrogen, the charge on Ni(II) is 1.045 e (Table 2). The electron density donation is much more pronounced in complexes with two ligands, leading to nickel ion charges of 1.045 (PLSC), 0.639 (PLTSC), and 0.916 e (PLITSC). In these complexes, the lowest charge is obtained for nitrogen atoms of the PLITSC ligand (−0.736 e), followed by oxygen (−0.637 e) and sulfur (−0.024 e). These charges further influence the complexes' bond lengths and stability, as discussed in the following section.

2.3. QTAIM Analysis

The QTAIM approach is based on Bader's theory of interacting atoms in molecules, and it is useful for examining metal–ligand interactions [26]. Within this approach, the topological properties of electron density and Laplacian in Bond Critical Points (BCPs) are calculated. In this section, the stabilization interactions between donor atoms and central metal ions are examined, along with the interactions formed between ligand molecules. The following parameters are included in the discussion: the electron density ($\rho(r)$), Laplacian ($\nabla^2\rho(r)$), Lagrangian kinetic electron density ($G(r)$), potential electron density ($V(r)$), density of total electron energy ($H(r) = G(r) + V(r)$), and interatomic bond energy ($E_{bond} = V(r)/2$), as presented in [33]. Based on the classification proposed by Bader and Essen, there are two types of interactions. Shared (covalent) interactions are characterized by a high electron density (>0.1 a.u.), while closed-shell regions (ionic bonds, van der Waals interactions, and hydrogen bonds) commonly have an electron density of around 0.01 a.u. [34]. These parameters are shown in Table 2 for the selected bonds, while the complete list is given in Table S4.

All Laplacian values are positive in the examined complexes, allowing for their characterization as electron-shared interactions [35]. Bianchi et al. proposed a more detailed bond regiment

based on the ratio of G(r) and V(r) into three categories: shared shell region of covalent bonds ($-$G(r)/V(r) > 2), intermediate (transit) region with dative bonds and ionic bonds of weak covalent degree (1 > $-$G(r)/V(r) > 2), and closed-shell region of ionic bonds and van der Walls interactions ($-$G(r)/V(r) < 1) [36]. Additionally, the bond degree is defined as the ratio between total electron energy and electron density (BD = H(r)/ρ(r)), or the total energy per electron [37]. The meaning of this parameter depends on the total energy density. If H > 0, the BD determines the softening degree of the non-covalent interaction. When H < 0, the parameter can be denoted as a covalent degree (CD), and a higher value indicates a stronger covalent feature [37,38]. The interactions between nitrogen, oxygen, sulfur atoms, and central metal ions have Laplacian values between 0.323 and 0.503 a.u. ([Ni(PLSC)(H_2O)$_3$]$^{2+}$), while the values of $-$G(r)/V(r) depend on the chosen atom. Three water molecules interact through bonds with weak covalent characters ($-$G(r)/V(r) = 1.1). On the other side, Ni–O_{aliph} falls within the same category, while Ni–O_{arom} and Ni–$N_{azomethine}$ can be classified as dative bonds with $-$G(r)/V(r) $\leq$ 1. This character is additionally proven by the negative total electron density value of the Ni–$N_{azomethine}$ bond. The degree of covalence character can be estimated by the Espinosa et al. approach of calculating the H(r)/ρ(r) parameter [39]. The value of this parameter for water molecules is 0.13 and 0.20, depending on its position. A water molecule in the same plane as the PLSC ligand has a lower H(r)/ρ(r) value. Where electronegative atoms of PLSC are concerned, the values are much lower, between 0.03 (Ni–O_{arom}) and 0.09 (Ni–O_{aliph}), proving a lower covalent character of these bonds than in the case of water molecules. The bond between nitrogen and Ni(II) has negative total energy, and the covalent degree is only -0.04. The interatomic bond energy nicely follows this discussion, as the strongest bond is formed with the aromatic oxygen atom ($-$160.3 kJ mol^{-1}), followed by azomethine nitrogen ($-$143.4 kJ mol^{-1}) and aliphatic oxygen ($-$118.2 kJ mol^{-1}) (Table 2 and Table S4). The structure of the ligand also contains a weak intermolecular hydrogen bond (C–H···O) with $-$G(r)/V(r) = 1.2 and bond energy of $-$16.9 kJ mol^{-1}.

Once the oxygen atom is exchanged with the sulfur atom, the interaction between sulfur and the central metal ion is characterized by electron density and Laplacian values of 0.054 and 0.190 a.u. (Table 3). These values, together with $-$G(r)/V(r) = 1 and negative total electron energy (Table 2), classify this interaction as dative or ionic. The covalent degree of Ni–S is higher than that of Ni–$N_{azomethine}$ ($-$0.07 vs. 0.01, Table S4). The interaction energy is lower ($-$72.4 kJ mol^{-1}) compared to Ni–O_{aliph}. This change is reflected in the increased bond distance, as previously discussed. Coordinated water molecules in [Ni(PLTSC)(H_2O)$_3$]$^{2+}$ have bonding energies of $-$80.4 and $-$103.4 kJ mol^{-1}, again depending on their position. It is important to observe that the parameters of Ni–O_{arom} and Ni–O_{aliph} are very similar to the first complex cation, although the interaction energies are lower for several kJ mol^{-1}. The interaction with the azomethine nitrogen atom still has negative total electron energy. The presence of the second donor nitrogen atom in the structure of [Ni(PLITSC)(H_2O)$_3$]$^{2+}$ affects the formation of a novel Ni–N_{amino} bond, with negative total energy ($-$10.2 kJ mol^{-1}) and an interaction energy of $-$141.0 kJ mol^{-1}. The CD parameter is lower when the amino group nitrogen atom is included. The bond energy in this structure is higher than that between azomethine nitrogen and Ni(II). When three different donor atoms (O_{aliph}, S, and N_{amino}) in complexes with three water molecules are compared, it can be concluded that the strongest interaction is formed with nitrogen, followed by oxygen and sulfur atoms. This is an expected order, bearing in mind the donating abilities of these atoms. These bonds have a pure dative or ionic character, with a slight contribution from covalent bonds in the case of oxygen atoms. These parameters influence the bond lengths from previous sections.

The structures of complex cations with two tridentate ligands were also analyzed. The parameters of interactions between donor atoms and the central metal ion in [Ni(PLSC)$_2$]$^{2+}$ are equal for two ligands, proving that a certain degree of symmetry exists in the structure. The interatomic bond energies of Ni–O_{arom} and Ni–O_{aliph} were lowered ($-$138.9 and $-$96.2 kJ mol^{-1}) compared to complex cation with one PLSC ligand, while the bond energy increased for Ni–$N_{azomethine}$ bond. The CD parameter of both bonds with azomethine nitrogen was the same ($-$0.04). This is a consequence of the bulkiness of ligands and their accommodation around

the central metal ion. When two PLTSC ligands are present, the bond energy of Ni–S is even lower (-59.6 kJ mol^{-1}), as expected for a structure with the longest donor atom–central metal ion bond. It should be outlined that the total electron density of Ni–N$_{azomethine}$ bonds is positive, with a low CD value of (0.002) compared to bonds with oxygen atoms (0.09). The same is found for the third bisligand complex, with the bond energy of Ni–N$_{amino}$ (-111.1 kJ mol^{-1}). The $-G(r)/V(r)$ ratio is the highest for oxygen atoms, signifying a slight covalent character, while only Ni–N$_{azomethine}$ has a negative total electron energy and the lowest covalent degree.

Table 3. The calculated Bond Critical Point (BCP) properties of selected bonds at the DFT/B3LYP-D3BJ/6-311+G(d,p)(H,C,N,O,S)/LanL2DZ(Ni) level of theory: the electron density ($\rho(r)$) and its Laplacian ($\nabla^2\rho(r)$); the Lagrangian kinetic electron density ($G(r)$) and the potential electron density ($V(r)$); the density of the total energy of electrons ($H(r)$)–Cremer–Kraka electronic energy density; the interatomic bond energy, E_{bond}.

Bond	$\rho(r)$ [a.u.]	$\nabla^2\rho(r)$ [a.u.]	$G(r)$ [kJ mol^{-1}]	$V(r)$ [kJ mol^{-1}]	$H(r)$ [kJ mol^{-1}]	$-G(r)/V(r)$	E_{bond} [kJ mol^{-1}]	$H(r)$ [a.u.]/$\rho(r)$ [a.u.]
[Ni(PLSC)(H$_2$O)$_3$]$^{2+}$								
Ni–O$_{aliph}$	0.059	0.404	250.8	-236.4	14.4	1.1	-118.2	0.09
[Ni(PLTSC)(H$_2$O)$_3$]$^{2+}$								
Ni–S	0.054	0.190	134.9	-144.7	-9.9	0.9	-72.4	-0.07
[Ni(PLITSC)(H$_2$O)$_3$]$^{2+}$								
Ni–N$_{amino}$	0.071	0.398	271.7	-282.0	-10.2	1.0	-141.0	-0.05
[Ni(PLSC)$_2$]$^{2+}$								
Ni–O$_{aliph}$ 1	0.052	0.347	210.1	-192.4	17.7	1.1	-96.2	0.13
Ni–O$_{aliph}$ 2	0.052	0.347	210.2	-192.5	17.7	1.1	-96.2	0.13
[Ni(PLTSC)$_2$]$^{2+}$								
Ni–S 1	0.047	0.168	114.8	-119.2	-4.4	1.0	-590.5	-0.04
Ni–S 2	0.047	0.167	114.3	-118.7	-4.4	1.0	-59.3	-0.04
[Ni(PLITSC)$_2$]$^{2+}$								
Ni–N$_{amino}$ 1	0.060	0.344	224.1	-222.3	1.9	1.0	-111.1	0.01
Ni–N$_{amino}$ 2	0.060	0.344	224.1	-222.2	1.9	1.0	-111.1	0.01

Another parameter for investigation of Ni–X (X=O, S, N) stability is the ellipticity index (ε). According to Bader's theory, the high value of this parameter signifies unstable bonds [40]. The values of ε from Table S4 are relatively low and in a narrow region (0.044–0.149), indicating the dynamic stability of these bonds [27]. The increase in ε value is a consequence of the electron delocalization and the increase in the π character of bonding [37]. When water-containing complexes are compared, the bond ellipticities are 0.140 (Ni–O$_{aliph}$), 0.101 (Ni–S), and 0.149 (Ni–N$_{amino}$) (Table S4). Higher ε values indicate deviations from cylindrical symmetry, which are less pronounced in bonds containing sulfur, which is a larger and less electronegative atom than nitrogen and oxygen. The reasons for the deviation from cylindrical symmetry include π-bonding or multiple bonding characters. The same trend was observed for complexes with two PLSC/PLTSC/PLITSC ligands. These results prove the assumption that the presence of different donor atoms influences the stability of compounds and that theoretical methods can be applied to predict compounds, even before their experimental preparation. This is an important finding, showing that that structures of known compounds can be used to estimate the stability and reactivity of novel ones, as discussed in [35].

2.4. Protein and DNA Binding Properties of Complexes

The examination of interactions between transport proteins/DNA and metal complexes is one of the common methods for predicting activity. Transport proteins are essential for distributing important compounds, such as fatty acids, metal ions, drugs, and

toxins [41,42]. Their interactions with DNA are considered one of the main pathways for the cytotoxic activity of compounds [43]. Several experimental and theoretical methodologies have been applied to examine similar compounds in the literature [16,17,23]. In this section, molecular docking simulations were performed to determine the affinity of selected complex cations towards protein and DNA binding. The most stable structures optimized at the B3LYP-D3BJ/6-311+G(d,p)(H,C,N,O,S)/LanL2DZ(Ni) level of theory were selected as flexible ligands, while the structures of HSA and DNA, obtained from the Cambridge Crystallographic Data Centre, were kept rigid.

The structure of HSA includes three domains (I, II, and III), further divided into two subdomains (A and B), leading to six subdomains, as shown in Figure 4. Peptide chains connect two subdomains within each domain, represented in light gray. The cavities of the subdomains include the fatty acid binding sites (FA) that are important for transporting fatty acids and other compounds. The fluorescence emission of HSA originates from Trp214 amino acid, located between domains IIA and IIB. The selected HSA structure contains six myristic acid molecules that mimic different fatty acids bound to transport proteins. Only the most stable conformations are discussed in the main text, while the complete list of molecular docking results is given in Table S5. Previous findings have shown that one of the chosen complex cations ($[Ni(PLTSC)_2]^{2+}$) bonded spontaneously to HSA and induced a decrease in the fluorescence intensity [17]. This result and the molecular docking simulation in the same reference verified that the binding position of compounds should be around Trp2014.
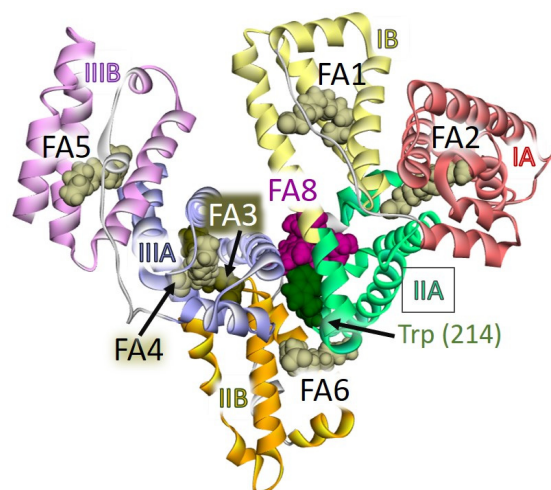

Figure 4. Structure of HSA with subdomains: IA in reddish, IB in yellow, IIA in green, IIB in orange, IIIA in lilac, and IIIB in pink. The active positions FA1–FA8 are denoted with the representation of myristic acids (yellow CPK model), commonly bound in the structures. The position of a fluorescent amino acid, Trp214, is depicted as dark green CPK balls, while $[Ni(PLSC)_2]^{2+}$ is presented as purple CPK balls.

Where interactions with HSA are concerned, examining the effect of ligands on the binding affinity is important. In the case of complex cations with three molecules of water, the changes in Gibbs free energy of binding are −24.6 ($[Ni(PLSC)(H_2O)_3]^{2+}$), −33.6 ($[Ni(PLTSC)(H_2O)_3]^{2+}$), and −26.2 kJ mol^{-1} ($[Ni(PLITSC)(H_2O)_3]^{2+}$). The most stable structures are formed within the FA8 site containing Trp214, as given in Table S5. A narrow range of values suggests that similar interactions were formed between amino acids and various ligands. Figure 5 (left) depicts the most important interactions with $[Ni(PLSC)(H_2O)_3]^{2+}$. There are classic hydrogen bonds with Glu153 and Glu291 in which both amino acids act as hydrogen atom acceptors in interactions with amino groups and water molecules. A weak hydrogen bond includes a hydrogen atom of an aliphatic chain of complex cations and Ser192/Glu188. Hydrophobic interactions between His288/Ala291 and the methyl group attached to the pyridine ring are present. A higher number of classic hydrogen bonds is found for $[Ni(PLTSC)(H_2O)_3]^{2+}$ (Figure S7), leading to the lowest ΔG_b value, comparable to the native ligand, warfarin (−34.0 kJ mol^{-1}). These interactions are

formed with Ser454, Ser202, Glu450, and electronegative groups (hydroxyl and amino) and water molecules. The presence of a sulfur atom in the ligand structure of PLTSC leads to the sulfur–π interaction with Trp214. Other weak interactions are hydrophobic (Val344 and Arg485) and carbon–hydrogen bonds (Ser454). Five hydrogen bonds with Asp451, Glu450, and Ser202 are included through interactions with water molecules and hydrogen attached to the pyridine nitrogen atom of $[Ni(PLITSC)(H_2O)_3]^{2+}$. The methylthio group is flexible and can form sulfur–π interactions, in this case, with Trp214 (Figure S7). The hydrophobic and carbon/π-donor hydrogen bonds additionally stabilize the investigated system. Based on these results, it can be concluded that the water molecules in the structures of complex cations are important for the formation of interactions with surrounding amino acids. At the same time, the sulfur atom introduces a different type of interaction that lowers the change in Gibbs free energy of binding.
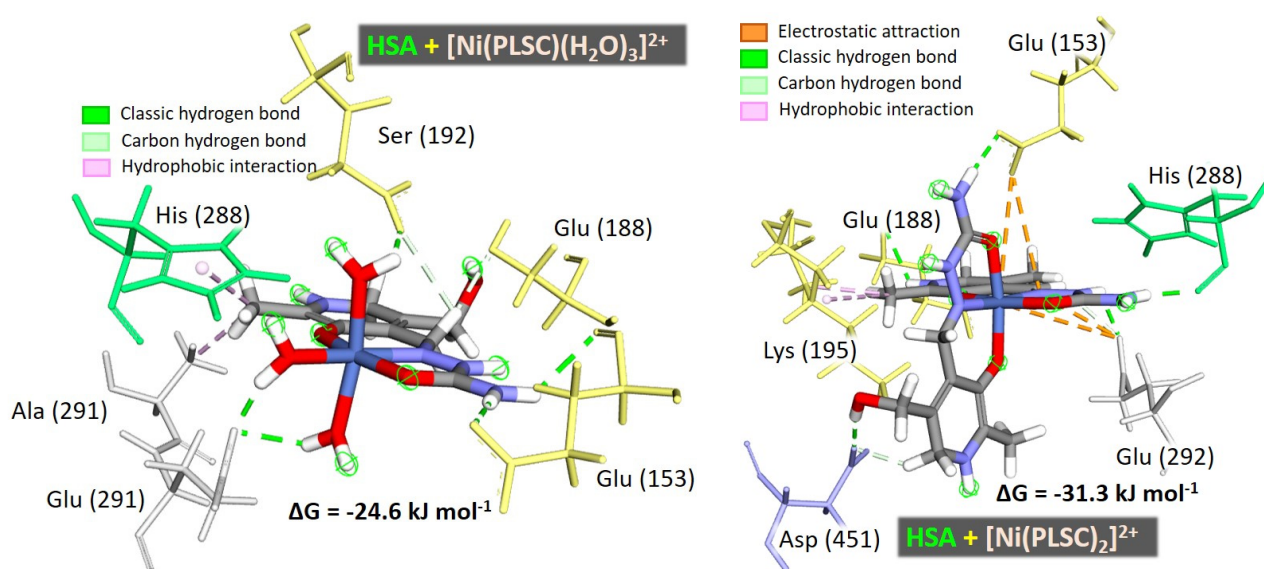
Figure 5. The most important interactions between HSA and $[Ni(PLSC)(H_2O)_3]^{2+}$ (**left**) and $[Ni(PLSC)_2]^{2+}$ (**right**) complexes, as obtained in the molecular docking simulations.

When two PLSC ligands are present in the structure, the value of ΔG_b is lowered to -31.3 kJ mol^{-1} due to the increased number of hydrogen bonds with His288, Glu292, Glu188, and Asp451. The electrostatic attraction is between the central metal ion and Glu153 and Glu292. The increase in the size of $[Ni(PLSC)_2]^{2+}$ compared to $[Ni(PLSC)(H_2O)_3]^{2+}$ allows for a higher number of strong interactions, especially hydrogen bonds. Additionally, alkyl interactions with Ala191 and Lys195 are shown in Figure 5. The binding energies of the other two complexes are lower than those of complex cations with three molecules of water, -25.9 and -26.1 kJ mol^{-1} for $[Ni(PLTSC)_2]^{2+}$ and $[Ni(PLITSC)_2]^{2+}$, respectively (Table S5 and Figure S8). The results from Table S5 also show that complex cations form interactions with amino acids within FA8. The multitude of amino groups is responsible for a high number of hydrogen bonds between amino acid residues and $[Ni(PLTSC)_2]^{2+}$. The lower binding affinities of these two complex cations can be explained by the existence of unfavorable interactions with His440 ($[Ni(PLTSC)_2]^{2+}$), Lys195, and Arg218 ($[Ni(PLITSC)_2]^{2+}$). His440 is also engaged in sulfur–π interactions with PLTSC ligands. In the case of PLITSC, two sulfur–π interactions include Asp451 and Arg222. These findings support the assumption that the selection of ending groups of the aliphatic chain has a profound effect on the binding affinity, along with the presence of sulfur atoms and aromatic structures.

The molecular docking simulations were performed for isolated PLSC, PLTSC, and PLITSC ligands to examine their binding positions and affinity towards HSA protein. The binding energies of these ligands were -26.7, -26.4, and -28.1 kJ mol^{-1} (Table S5),

respectively. These values were comparable to the values obtained for complexes with two tridentate ligands, thus proving the importance of ligand structures for the binding of complexes. An important difference in these cases was the binding site. Namely, all three ligands were bound to the active sites IB and IIA due to their size (Figure S9). The elongated structure of ligands with several polar groups allowed for the formation of several hydrogen bonds, all presented in Figure S10. All three ligands were positioned further from the Trp214 amino acid than the respective complexes.

During molecular docking simulations, several positions were obtained for the interactions between complex cations and DNA. For example, 13 different orientations were found for $[Ni(PLSC)(H_2O)_3]^{2+}$, with changes in Gibbs free energy of binding of between −35.9 and −26.8 kJ mol^{-1}. Some of these positions are depicted in Figure S11, denoted by the changes in Gibbs free energies ΔG_1, ΔG_6, ΔG_7, and ΔG_{10}. It should be mentioned that each of these positions included several orientations of the complex cation within the DNA structure. The most stable conformation is presented in Figure 6. There are several hydrogen bonds between water molecules and the oxygen and nitrogen atoms of a phosphate group, sugar, and aromatic rings. PLSC ligands also interact with the oxygen atoms of aromatic rings and sugars through hydroxymethyl oxygen, amino, and azomethine nitrogens. The change in Gibbs energy of binding is the lowest among the investigated complex cations (−35.9 kJ mol^{-1}, Table S6) due to the positions of electronegative groups in the minor groove of DNA. The number of hydrogen bonds is lowered in the complex cations with three molecules of water and PLTSC/PLITSC ligands, leading to binding energies of −31.9 and −31.3 kJ mol^{-1}. As presented in Figure S12, eight and seven classic hydrogen bonds exist between water molecules and the hydroxyl group of ligands on one side and oxygen atoms of sugars and aromatic rings. These hydrophobic interactions include the methyl groups of PLTSC/PLITSC and the aromatic rings of guanine and cytosine in positions 10, 11, 14, and 15.
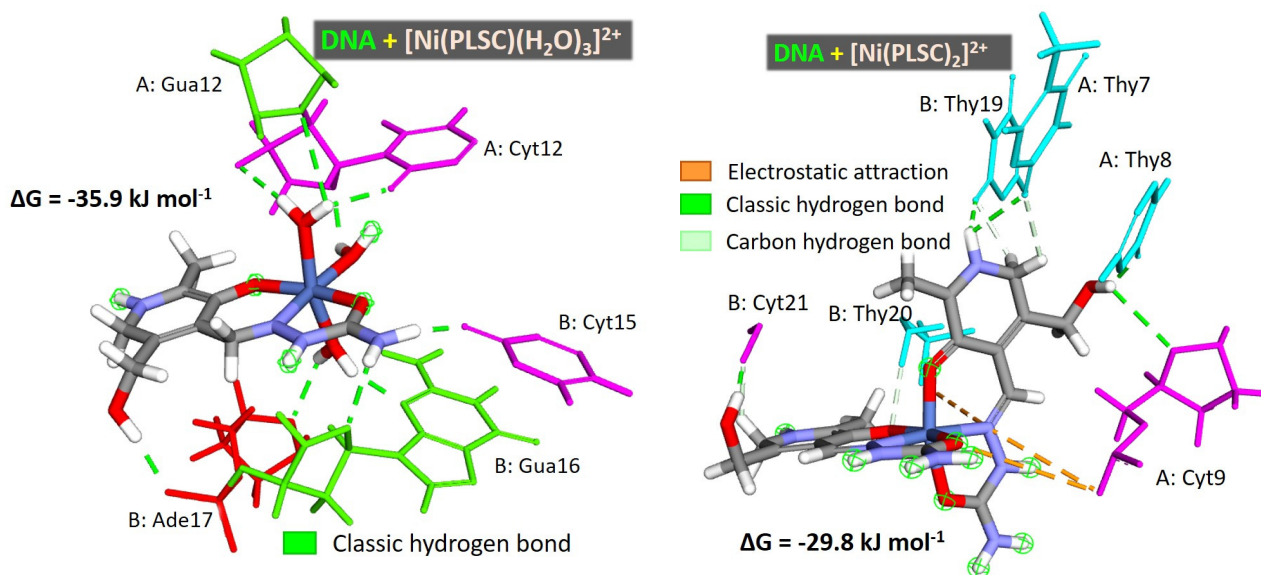

Figure 6. The most important interactions between DNA and $[Ni(PLSC)(H_2O)_3]^{2+}$ (**left**) and $[Ni(PLSC)_2]^{2+}$ (**right**) complexes, as obtained via the molecular docking simulations.

Removing water molecules from complex cations lowers the change in Gibbs free binding energy for several kJ mol^{-1}, although novel interactions are introduced. In the case of $[Ni(PLSC)_2]^{2+}$, the number of classic hydrogen bonds is reduced to five (Figure 6), and the change in Gibbs free energy of binding is −29.8 kJ mol^{-1}. Electrostatic interactions between the positively charged pyridine nitrogen and azomethine nitrogen of PLSC and the negatively charged oxygen atoms of the phosphate groups of cytosine and thymine can be observed. Carbon hydrogen bonds also exist with thymine residues in positions 7 and 19 and cytosine residues in position 21. The binding of $[Ni(PLTSC)_2]^{2+}$ and $[Ni(PLITSC)_2]^{2+}$ is even less spontaneous: −26.8 and −28.7 kJ mol^{-1}. The same types of interactions are presented in Figure S13, as previously discussed. Therefore, the

binding to DNA is guided by water molecules, leading to a much more spontaneous process. When three ligands are compared, the ending amino group and oxygen atom in the PLSC ligand are responsible for the highest number of hydrogen bonds. The sulfur atom in the structure is excluded from these interactions due to low electronegativity and protection by the methyl group in the PLITSC ligand. The most important result is that all the analyzed complex cations bind in the minor groove of DNA, as the octahedral geometry limits other mechanisms.

The interactions between DNA and free ligands were also investigated, and the binding energies are presented in Table S6. These energies were −26.7 (PLSC), −26.4 (PLITSC), and −28.6 kJ mol^{-1} (PLITSC). All free ligands were located in the minor groove of the DNA, which coincides with their respective complexes. The binding energies were lower than for the complexes with three water molecules, concluding that they were important for the system's stability. Complexes with two tridentate ligands showed affinity almost equal to the free ligands. The most important interactions are depicted in Figure S14. Due to the presence of electronegative groups, the number of classic hydrogen bonds was five (PLTSC and PLITSC) and eight (PLTSC), similar to the binding of complex cations. Free PLSC ligands and two complexes showed the highest binding affinity towards DNA. The experimental examination of DNA affinity and interactions in vivo is recommended to verify these theoretical findings, as additional ions and solvent molecules might influence these processes.

3. Materials and Methods

3.1. Hirshfeld Surface Analysis

The Hirshfeld surface analysis was applied to investigate the intramolecular interactions responsible for the stabilization of the crystal structure. The CrystalExplorer program [44] was utilized for this analysis. The results are represented by a graph connecting two distances: one between the two nearest nuclei (d_e) and the second between the nuclei and the external surface (d_i) [45,46]. The distance values are normalized and colored depending on the sum of the van der Waals radii of the interacting atoms. Red, white, and blue colors are used for the shorter, equal, and longer separations than the respective van der Walls radii. The specific contacts are shown in fingerprint plots that allow for the determination of their percentages in the total number of contacts. The crystallographic structures of four Ni(II) nitrate complexes with the mentioned ligands are taken from the Cambridge Crystallographic Data Centre (CCDC), as given in the following section. A similar analysis was previously discussed for PLSC, PLTSC, and PLITSC ligands with various transition metals [17,47].

3.2. Quantum-Chemical Analysis

The structures of the complex cations [Ni(PLSC)(H$_2$O)$_3$]$^{2+}$, [Ni(PLISC)$_2$]$^{2+}$, [Ni(PLTSC)(H$_2$O)$_3$]$^{2+}$, and [Ni(PLSC)2]$^{2+}$ were taken from crystallographic structures of their nitrate salts from references [12,18,19]. Additionally, two structures, [Ni(PLTSC)$_2$]$^{2+}$ and [Ni(PLITSC)(H$_2$O)$_3$]$^{2+}$, were prepared based on the structural parameters of similar compounds. The structures were optimized using the Gaussian 09 Program package [48] at the B3LYP/6-311++G(d,p)(H,C,N,O,S)/LanL2DZ(Ni) level of theory [49–52]. The same level of theory was previously applied for the optimization, spectral prediction, and reactivity description of other Ni(II) complexes [53–55]. The geometry optimization was performed without any geometrical constraints for the octahedral geometry, with a charge of +2 and a multiplicity of 3, corresponding to the common multiplicity of nickel-containing compounds. The absence of imaginary frequencies proved that the minimum on the potential energy surface was found. Counterpose (CP) corrections were applied to all binding energy values to minimize the basis set superposition error [56]. The natural bond orbital charges were calculated using the NBO analysis approach [57], as implemented in the Gaussian 09. The Quantum Theory of Atoms in Molecules (QTAIM) analysis, as proposed by Bader [58,59], was performed using the AIMAll program (aim.tkgristmill.com) package [60]. Different parameters calculated from the total electron energy contributions are described in the main text.

3.3. Molecular Docking

Molecular-level investigations into the binding interactions between nickel(II) complexes, human serum albumin (HSA), and deoxyribonucleic acid (DNA) were performed using molecular docking simulations with AutoDock 4.2.6 [61], facilitated by the AMDock program (version 1.5.2) [62]. The structures of all six nickel(II) coordination complexes were optimized using the Gaussian 09 Program package at the B3LYP-D3BJ/6-311+G(d,p)(H,C,N,O,S)/ LanL2DZ(Ni) level of theory. The structures of HSA (PDB ID: 1H9Z [63]) and DNA (PDB ID: 1BNA [64]) were retrieved from the Protein Data Bank (PDB). The number of poses was set to 20, the number of runs was set to 100, and the energy evaluations were set to 10,000,000. BIOVIA Discovery Studio was employed for molecular preparation and the docking setup and for visualizing and analyzing the docking results.

4. Conclusions

The most numerous contacts in the crystal structures of $[Ni(PLSC)(H_2O)_3]\cdot 2NO_3^-$, $[Ni(PLTSC)_2]\cdot 2NO_3^-\cdot H_2O$, and $[Ni(PLITSC)(H_2O)_3]\cdot 2NO_3^-$ are denoted as O⋯H, with the following percentages: 49.1, 36.3, and 43.8. A significant part of these interactions is due to three molecules of water. When PLTSC and PLITSC are part of the structure, the sulfur atom is included in S⋯H, S⋯C, S⋯O, and S⋯N contacts. Important stabilization interactions also exist between protonated nitrogen atoms and surrounding electronegative groups. The optimized structures of the three mentioned complexes were performed at the B3LYP/6-311++G(d,p)(H,C,N,O,(S))/LanL2DZ(Ni) level of theory. The correlation coefficients for bond length comparisons are between 0.96 and 0.99, with MAE values between 0.017 and 0.041 Å. The bond angles are also well reproduced, with correlation coefficients of 0.99 and MAE values between 1.50 and 1.94°. Upon optimization, the structures adopted almost perfect octahedral geometry. The structures of the other three complex cations were optimized at the same level of theory. The highest binding energy (941 kJ mol^{-1}) was calculated for the PLSC ligand due to the existence of oxygen and nitrogen donor atoms. Where complex cations with two PLSC/PLTSC/PLITSC ligands are concerned, the highest binding energy was obtained for $[Ni(PLITSC)_2]^{2+}$, in which two to three nitrogen atoms of each ligand surround the central metal ion. The NBO charge analysis proved that significant donations from ligands to the Ni(II) orbitals existed. The interactions between donor atoms and Ni(II) were further examined using the QTAIM approach. The strongest interaction, as determined by the interatomic bond energy, was between the nitrogen atom of the amino group of PLITSC (−140.0 kJ mol^{-1}), followed by the oxygen atom of PLSC (−118.2 kJ mol^{-1}) and the sulfur atom of PLTSC (−72.4 kJ mol^{-1}). All the bonds showed a partial covalent character, especially with oxygen atoms. The same trend was found in the complexes with two ligands. The HSA binding affinity was also dependent on the ligands. All complex cations were positioned close to the fluorescent amino acid Trp214 in the most stable structures. The most important interactions included classic hydrogen bonds, carbon–hydrogen bonds, and hydrophobic interactions. The structures of PLTSC and PLITSC allowed for the formation of sulfur–π interactions. The binding energy of $[Ni(PLTSC)(H_2O)_3]^{2+}$ was comparable to warfarin, a native ligand in the examined crystal structure. The most stable position for the interactions with DNA was in the minor groove, which was expected due to the size and geometry of the complexes. The highest affinity towards DNA was calculated for two complex cations with the PLSC ligand due to the spatial distribution of electronegative groups interacting with nucleobases. Further experimental studies are recommended to obtain the binding constants and to examine the influence of solvent molecules and types of interactions between biomolecules and nickel(II) complexes.

$[Ni(PLTSC)(H_2O)_3]^{2+}$ with atom numbering scheme; Table S1: Experimental and theoretical (at the B3LYP/6-311++G(d,p)(H,C,N,O)/LanL2DZ(Ni) level of theory) bond lengths (Å) and angles (°) in the structure of $[Ni(PLSC)(H_2O)_3]^{2+}$; Figure S5: Optimized structure of $[Ni(PLITSC)(H_2O)_3]^{2+}$ with atom numbering scheme; Table S2: Experimental and theoretical (at the B3LYP/6-311++G(d,p)(H,C,N,O,S)/LanL2DZ(Ni) level of theory) bond lengths (Å) and angles (°) in the structure of $[Ni(PLITSC)(H_2O)_3]^{2+}$; Figure S6: Optimized structure of $[Ni(PLTSC)_2]^{2+}$ with atom numbering scheme; Table S3: Experimental and theoretical (at the B3LYP/6-311++G(d,p)(H,C,N,O,S)/LanL2DZ(Ni) level of theory) bond lengths (Å) and angles (°) in the structure of $[Ni(PLTSC)_2]^{2+}$; Table S4: The calculated Bond Critical Point (BCP) properties at the DFT/B3LYP-D3BJ/6-311+G(d,p)/def2-TZVP level of theory: the electron density ($\rho(r)$) and its Laplacian ($\nabla^2\rho(r)$); the Lagrangian kinetic electron density ($G(r)$) and the potential electron density ($V(r)$); the density of the total energy of electrons ($H(r)$)–Cremer–Kraka electronic energy density; the interatomic bond energy, E_{bond}, ε–ellipticity parameter; Table S5: Binding energies, sites, and number of runs for the selected Ni(II) complexes, warfarin, and HAS, as obtained via the molecular docking simulations; Figure S7: The most important interactions between HSA and $[Ni(PLTSC)(H_2O)_3]^{2+}$ (left) and $[Ni(PLITSC)(H_2O)_3]^{2+}$ (right) complexes, as obtained via the molecular docking simulations; Figure S8: The most important interactions between HSA and $[Ni(PLTSC)_2]^{2+}$ (left) and $[Ni(PLITSC)_2]^{2+}$ (right) complexes, as obtained via the molecular docking simulations; Figure S9: The binding positions of PLITSC, $[Ni(PLITSC)(H_2O)_3]^{2+}$, and $[Ni(PLITSC)_2]^{2+}$ within the structure of HAS; Figure S10: The most important interactions between HSA and PLSC, PLTSC, and PLITSC ligands, as obtained via the molecular docking simulations; Table S6: Binding energies, sites, and number of runs for the selected Ni(II) complexes, warfarin, and HAS, as obtained via the molecular docking simulations; Figure S11: Different docking positions of $[Ni(PLSC)(H_2O)_3]^{2+}$ in the structure of DNA; Figure S12: The most important interactions between DNA and $[Ni(PLTSC)(H_2O)_3]^{2+}$ (left) and $[Ni(PLITSC)(H_2O)_3]^{2+}$ (right) complexes, as obtained via the molecular docking simulations; Figure S13: The most important interactions between DNA and $[Ni(PLTSC)_2]^{2+}$ (left) and $[Ni(PLITSC)_2]^{2+}$ (right) complexes, as obtained via the molecular docking simulations; Figure S14: The most important interactions between HSA and PLSC, PLTSC, and PLITSC ligands, as obtained via the molecular docking simulations.

References

1. Barone, G.; Terenzi, A.; Lauria, A.; Almerico, A.M.; Leal, J.M.; Busto, N.; García, B. DNA-binding of nickel(II), copper(II) and zinc(II) complexes: Structure–affinity relationships. *Coord. Chem. Rev.* **2013**, *257*, 2848–2862. [CrossRef]
2. Jamieson, E.R.; Lippard, S.J. Structure, Recognition, and Processing of Cisplatin–DNA Adducts. *Chem. Rev.* **1999**, *99*, 2467–2498. [CrossRef] [PubMed]
3. Todd, R.C.; Lippard, S.J. Inhibition of transcription by platinum antitumor compounds. *Metallomics* **2009**, *1*, 280. [CrossRef] [PubMed]
4. Busto, N.; Valladolid, J.; Martínez-Alonso, M.; Lozano, H.J.; Jalón, F.A.; Manzano, B.R.; Rodríguez, A.M.; Carrión, M.C.; Biver, T.; Leal, J.M.; et al. Anticancer Activity and DNA Binding of a Bifunctional Ru(II) Arene Aqua-Complex with the 2,4-Diamino-6-(2-pyridyl)-1,3,5-triazine Ligand. *Inorg. Chem.* **2013**, *52*, 9962–9974. [CrossRef]
5. Sigel, A.; Sigel, H.; Sigel, R.K.O. (Eds.) *Nickel and Its Surprising Impact in Nature*; Wiley: Hoboken, NJ, USA, 2007; ISBN 9780470016718.

6. Alper, P.; Erkisa, M.; Genckal, H.M.; Sahin, S.; Ulukaya, E.; Ari, F. Synthesis, characterization, anticancer and antioxidant activity of new nickel(II) and copper(II) flavonoid complexes. *J. Mol. Struct.* **2019**, *1196*, 783–792. [CrossRef]

7. Wu, H.; Yuan, J.; Bai, Y.; Pan, G.; Wang, H.; Shu, X. Synthesis, structure, DNA-binding properties and antioxidant activity of a nickel(II) complex with bis(N-allylbenzimidazol-2-ylmethyl)benzylamine. *J. Photochem. Photobiol. B Biol.* **2012**, *107*, 65–72. [CrossRef]

8. Maia, D.O.; Santos, V.F.; Barbosa, C.R.S.; Fróes, Y.N.; Muniz, D.F.; Santos, A.L.E.; Santos, M.H.C.; Silva, R.R.S.; Silva, C.G.L.; Souza, R.O.S.; et al. Nickel(II) chloride schiff base complex: Synthesis, characterization, toxicity, antibacterial and leishmanicidal activity. *Chem. Biol. Interact.* **2022**, *351*, 109714. [CrossRef]

9. Alomar, K.; Landreau, A.; Allain, M.; Bouet, G.; Larcher, G. Synthesis, structure and antifungal activity of thiophene-2,3-dicarboxaldehyde bis(thiosemicarbazone) and nickel(II), copper(II) and cadmium(II) complexes: Unsymmetrical coordination mode of nickel complex. *J. Inorg. Biochem.* **2013**, *126*, 76–83. [CrossRef] [PubMed]

10. Pelosi, G.; Bisceglie, F.; Bignami, F.; Ronzi, P.; Schiavone, P.; Re, M.C.; Casoli, C.; Pilotti, E. Antiretroviral Activity of Thiosemicarbazone Metal Complexes. *J. Med. Chem.* **2010**, *53*, 8765–8769. [CrossRef]

11. Talib, J.; Harman, D.G.; Dillon, C.T.; Aldrich-Wright, J.; Beck, J.L.; Ralph, S.F. Does the metal influence non-covalent binding of complexes to DNA? *Dalt. Trans.* **2009**, *3*, 504–513. [CrossRef]

12. Leovac, V.M.; Jovanović, L.S.; Jevtović, V.S.; Pelosi, G.; Bisceglie, F. Transition metal complexes with thiosemicarbazide-based ligand—Part LV: Synthesis and X-ray structural study of novel Ni(II) complexes with pyridoxal semicarbazone and pyridoxal thiosemicarbazone. *Polyhedron* **2007**, *26*, 2971–2978. [CrossRef]

13. Leovac, V.M.; Jevtović, V.S.; Jovanović, L.S.; Bogdanović, G.A. Metal complexes with schiff-base ligands—Pyridoxal and semicarbazide-based derivatives. *J. Serbian Chem. Soc.* **2005**, *70*, 393–422. [CrossRef]

14. West, D.X.; Liberta, A.E.; Padhye, S.B.; Chikate, R.C.; Sonawane, P.B.; Kumbhar, A.S.; Yerande, R.G. Thiosemicarbazone complexes of copper(II): Structural and biological studies. *Coord. Chem. Rev.* **1993**, *123*, 49–71. [CrossRef]

15. Lobana, T.S.; Butcher, R.J. Metal—Thiosemicarbazone interactions. Synthesis of an iodo-bridged dinuclear [diiodobis(pyrrole-2-carbaldehydethiosemicarbazone)dicopper(I)] complex. *Transit. Met. Chem.* **2004**, *29*, 291–295.

16. Jevtovic, V.; Golubović, L.; Alshammari, B.; Alshammari, M.R.; Rajeh, S.Y.; Alreshidi, M.A.; Alshammari, O.A.O.; Rakić, A.; Dimić, D. Crystal Structure, Theoretical Analysis, and Protein/DNA Binding Activity of Iron(III) Complex Containing Differently Protonated Pyridoxal–S-Methyl-Isothiosemicarbazone Ligands. *Int. J. Mol. Sci.* **2024**, *25*, 7058. [CrossRef]

17. Jevtovic, V.; Alshamari, A.K.; Milenković, D.; Dimitrić Marković, J.; Marković, Z.; Dimić, D. The Effect of Metal Ions (Fe, Co, Ni, and Cu) on the Molecular-Structural, Protein Binding, and Cytotoxic Properties of Metal Pyridoxal-Thiosemicarbazone Complexes. *Int. J. Mol. Sci.* **2023**, *24*, 11910. [CrossRef]

18. Leovac, V.M.; Jovanović, L.S.; Divjaković, V.; Pevec, A.; Leban, I.; Armbruster, T. Transition metal complexes with thiosemicarbazide-based ligands. Part LIV. Nickel(II) complexes with pyridoxal semi- (PLSC) and thiosemicarbazone (PLTSC). Crystal and molecular structure of [Ni(PLSC)(H$_2$O)$_3$](NO$_3$)$_2$ and [Ni(PLTSC-H)py]NO$_3$. *Polyhedron* **2007**, *26*, 49–58. [CrossRef]

19. Jevtovic, V.; Vidovic, D. Synthesis, characterization and X-Ray crystal structure of the tri aqua (3-Hydroxy-5-Hydroxymethyl-2-Methylpyridine-4-Carboxaldehyde-3-Methylisotiosemicarbazone: K3, O3, N7, N10) Ni(II) nitrate. *J. Chem. Crystallogr.* **2010**, *40*, 794–798. [CrossRef]

20. Jevtovic, V.; Alshammari, N.; Latif, S.; Alsukaibi, A.K.D.; Humaidi, J.; Alanazi, T.Y.A.; Abdulaziz, F.; Matalka, S.I.; Pantelić, N.Đ.; Marković, M.; et al. Synthesis, Crystal Structure, Theoretical Calculations, Antibacterial Activity, Electrochemical Behavior, and Molecular Docking of Ni(II) and Cu(II) Complexes with Pyridoxal-Semicarbazone. *Molecules* **2022**, *27*, 6322. [CrossRef]

21. Ferrari Belicchi, M.; Fava Gasparri, G.; Leporati, E.; Pelizzi, C.; Tarasconi, P.; Tosi, G. Thiosemicarbazones as co-ordinating agents. Solution chemistry and X-ray structure of pyridoxal thiosemicarbazone trihydrate and spectroscopic properties of its metal complexes. *J. Chem. Soc. Dalt. Trans.* **1986**, *3*, 2455–2461.

22. Leovac, V.M.; Marković, S.; Divjaković, V.; Szécsényi, K.M.; Joksović, M.D.; Lebanc, I. Structural and DFT studies on molecular structure of Ni(II) chloride complex with pyridoxal semicarbazone (PLSC). Unusual coordination mode of PLSC. *Acta Chim. Slov.* **2008**, *55*, 850–860.

23. Jevtovic, V.; Alhar, M.S.O.; Milenković, D.; Marković, Z.; Dimitrić Marković, J.; Dimić, D. Synthesis, Structural Characterization, Cytotoxicity, and Protein/DNA Binding Properties of Pyridoxylidene-Aminoguanidine-Metal (Fe, Co, Zn, Cu) Complexes. *Int. J. Mol. Sci.* **2023**, *24*, 14745. [CrossRef] [PubMed]

24. Alshammari, O.A.O.; Maisara, S.; Alshammari, B.; Alshammari, M.R.; Rakic, V.; Dimitrić Marković, J.; Jevtovic, V.; Dimić, D. Theoretical Insights into Different Complexation Modes of Dioxovanadium(V) Compounds with Pyridoxal Semicarbazone/Thiosemicarbazone/S-Methyl-iso-thiosemicarbazone Ligands. *Molecules* **2024**, *29*, 1213. [CrossRef] [PubMed]

25. Gak Simić, K.; Đorđević, I.; Lazić, A.; Radovanović, L.; Petković-Benazzouz, M.; Rogan, J.; Trišović, N.; Janjić, G. On the supramolecular outcomes of fluorination of cyclohexane-5-spirohydantoin derivatives. *CrystEngComm* **2021**, *23*, 2606–2622. [CrossRef]

26. Gall, M.; Breza, M. QTAIM study of transition metal complexes with cyclophosphazene-based multisite ligands I: Zinc(II) and nickel(II) complexes. *Polyhedron* **2009**, *28*, 521–524. [CrossRef]

27. Karaush, N.N.; Baryshnikov, G.V.; Minaeva, V.A.; Minaev, B.F. A DFT and QTAIM study of the novel d-block metal complexes with tetraoxa[8]circulene-based ligands. *New J. Chem.* **2015**, *39*, 7815–7821. [CrossRef]

28. Caramori, G.F.; Parreira, R.L.T.; Ferreira, A.M.D.C. Isatin-Schiff base copper(II) complexes—A DFT study of the metal-ligand bonding situation. *Int. J. Quantum Chem.* **2012**, *112*, 625–646. [CrossRef]

29. Pitchumani Violet Mary, C.; Shankar, R.; Vijayakumar, S. Theoretical insights into the metal chelating and antimicrobial properties of the chalcone based Schiff bases. *Mol. Simul.* **2019**, *45*, 636–645. [CrossRef]

30. Kargar, H.; Ashfaq, M.; Fallah-Mehrjardi, M.; Behjatmanesh-Ardakani, R.; Munawar, K.S.; Tahir, M.N. Unsymmetrical Ni(II) Schiff base complex: Synthesis, spectral characterization, crystal structure analysis, Hirshfeld surface investigation, theoretical studies, and antibacterial activity. *J. Mol. Struct.* **2022**, *1265*, 133381. [CrossRef]

31. Guelai, A.; Brahim, H.; Guendouzi, A.; Boumediene, M.; Brahim, S. Structure, electronic properties, and NBO and TD-DFT analyses of nickel(II), zinc(II), and palladium(II) complexes based on Schiff-base ligands. *J. Mol. Model.* **2018**, *24*, 301. [CrossRef]

32. Dikmen, G.; Kani, İ. Synthesis, spectroscopic characterization (FT-IR, Raman, UV-VIS, XRD), DFT studies and DNA binding properties of [Ni(C$_6$H$_5$CH$_2$COO)(C$_{12}$H$_8$N$_2$)$_2$](ClO$_4$)(CH$_3$OH) compound. *J. Mol. Struct.* **2020**, *1209*, 127955. [CrossRef]

33. Kasalović, M.P.; Jelača, S.; Milanović, Ž.; Maksimović-Ivanić, D.; Mijatović, S.; Lađarević, J.; Božić, B.; Marković, Z.; Dunđerović, D.; Rüffer, T.; et al. Novel triphenyltin(iv) compounds with carboxylato *N*-functionalized 2-quinolones as promising potential anticancer drug candidates: In vitro and in vivo evaluation. *Dalt. Trans.* **2024**, *53*, 8298–8314. [CrossRef]

34. Soliman, S.M.; Albering, J.; Abu-Youssef, M.A.M. Structural analyses of two new highly distorted octahedral copper(II) complexes with quinoline-type ligands; Hirshfeld, AIM and NBO studies. *Polyhedron* **2017**, *127*, 36–50. [CrossRef]

35. Lepetit, C.; Vabre, B.; Canac, Y.; Alikhani, M.E.; Zargarian, D. Pentacoordinated, square pyramidal cationic PCP Ni(II) pincer complexes: ELF and QTAIM topological analyses of nickel–triflate interactions. *Theor. Chem. Acc.* **2018**, *137*, 141. [CrossRef]

36. Bianchi, R.; Gervasio, G.; Marabello, D. Experimental Electron Density Analysis of Mn 2 (CO) 10: Metal–Metal and Metal–Ligand Bond Characterization. *Inorg. Chem.* **2000**, *39*, 2360–2366. [CrossRef]

37. Sánchez-Coronilla, A.; Sánchez-Márquez, J.; Zorrilla, D.; Martín, E.I.; de los Santos, D.M.; Navas, J.; Fernández-Lorenzo, C.; Alcántara, R.; Martín-Calleja, J. Convergent study of Ru–ligand interactions through QTAIM, ELF, NBO molecular descriptors and TDDFT analysis of organometallic dyes. *Mol. Phys.* **2014**, *112*, 2063–2077. [CrossRef]

38. Uribe, E.A.; Daza, M.C.; Villaveces, J.L.; Delgado, S.A. On the nature of copper–hydrogen bonding: AIM and NBO analysis of CuH$_n$ ($1 \leq n \leq 6$) complexes. *Int. J. Quantum Chem.* **2010**, *110*, 524–531. [CrossRef]

39. Espinosa, E.; Alkorta, I.; Elguero, J.; Molins, E. From weak to strong interactions: A comprehensive analysis of the topological and energetic properties of the electron density distribution involving X–H···F–Y systems. *J. Chem. Phys.* **2002**, *117*, 5529–5542. [CrossRef]

40. Bader, R.F.W.; Slee, T.S.; Cremer, D.; Kraka, E. Description of conjugation and hyperconjugation in terms of electron distributions. *J. Am. Chem. Soc.* **1983**, *105*, 5061–5068. [CrossRef]

41. Fasano, M.; Curry, S.; Terreno, E.; Galliano, M.; Fanali, G.; Narciso, P.; Notari, S.; Ascenzi, P. The extraordinary ligand binding properties of human serum albumin. *IUBMB Life (Int. Union Biochem. Mol. Biol. Life)* **2005**, *57*, 787–796. [CrossRef]

42. Fanali, G.; di Masi, A.; Trezza, V.; Marino, M.; Fasano, M.; Ascenzi, P. Human serum albumin: From bench to bedside. *Mol. Asp. Med.* **2012**, *33*, 209–290. [CrossRef]

43. Palchaudhuri, R.; Hergenrother, P.J. DNA as a target for anticancer compounds: Methods to determine the mode of binding and the mechanism of action. *Curr. Opin. Biotechnol.* **2007**, *18*, 497–503. [CrossRef]

44. Turner, M.J.; McKinnon, J.J.; Wolff, S.K.; Grimwood, D.J.; Spackman, P.R.; Jayatilaka, D.; Spackman, M.A. *CrystalExplorer17*; University of Western Australia: Perth, Australia, 2017.

45. Spackman, M.A.; Jayatilaka, D. Hirshfeld surface analysis. *CrystEngComm* **2009**, *11*, 19–32. [CrossRef]

46. Spackman, M.A.; Byrom, P.G. A novel definition of a molecule in a crystal. *Chem. Phys. Lett.* **1997**, *267*, 215–220. [CrossRef]

47. Abdulaziz, F.; Alabbosh, K.F.; Alshammari, O.A.O.; Bin Tuwalah, W.M.; Alanazi, T.Y.A.; Rakić, A.; Barić, M.; Marković, M.; Jevtovic, V.; Dimić, D. Crystallographic Structure and Quantum-Chemical Analysis of Biologically Active Co(III)-Pyridoxal–Isothiosemicarbazone Complex. *Inorganics* **2023**, *11*, 466. [CrossRef]

48. Frisch, M.J.; Trucks, G.W.; Schlegel, H.B.; Scuseria, G.E.; Robb, M.A.; Cheeseman, J.R.; Scalmani, G.; Barone, V.; Mennucci, B.; Petersson, G.A.; et al. *Gaussian 09*; Gaussian Inc.: Wallingford, CT, USA, 2009.

49. Becke, A.D. Density-functional thermochemistry. III. The role of exact exchange. *J. Chem. Phys.* **1993**, *98*, 5648–5652. [CrossRef]

50. Dunning, T.H. Gaussian basis sets for use in correlated molecular calculations. I. The atoms boron through neon and hydrogen. *J. Chem. Phys.* **1989**, *90*, 1007. [CrossRef]

51. Hay, P.J.; Wadt, W.R. Ab initio effective core potentials for molecular calculations. Potentials for K to Au including the outermost core orbitale. *J. Chem. Phys.* **1985**, *82*, 299–310. [CrossRef]

52. Hay, P.J.; Wadt, W.R. Ab initio effective core potentials for molecular calculations. Potentials for the transition metal atoms Sc to Hg. *J. Chem. Phys.* **1985**, *82*, 270–283. [CrossRef]

53. Macit, M.; Tanak, H.; Orbay, M.; Özdemir, N. Synthesis, crystal structure, spectroscopic characterization and DFT studies of bis[(1Z,2E)-N-(2,6-diethylphenyl)-N'-hydroxy-2-(hydroxyimino)acetimidamidato]nickel(II). *Inorg. Chim. Acta* **2017**, *459*, 36–44. [CrossRef]

54. Genc, Z.K.; Tekin, S.; Sandal, S.; Sekerci, M.; Genc, M. Synthesis and DFT studies of structural and some spectral parameters of nickel(II) complex with 2-(2-hydroxybenzoyl)-N-(1-adamantyl) hydrazine carbothioamide. *Res. Chem. Intermed.* **2015**, *41*, 4477–4488. [CrossRef]

55. Rahnamaye Aliabad, H.A.; Chahkandi, M. Optoelectronic and structural studies of a Ni(II) complex including bicyclic guanidine ligands: DFT calculations. *Comput. Theor. Chem.* **2017**, *1122*, 53–61. [CrossRef]

56. Boys, S.F.; Bernardi, F. The calculation of small molecular interactions by the differences of separate total energies. Some procedures with reduced errors. *Mol. Phys.* **1970**, *19*, 553–566. [CrossRef]

57. Reed, A.E.; Weinstock, R.B.; Weinhold, F. Natural population analysis. *J. Chem. Phys.* **1985**, *83*, 735–746. [CrossRef]

58. Bader, R.F.W. Atoms in molecules. *Acc. Chem. Res.* **1985**, *18*, 9–15. [CrossRef]

59. Bader, R.F.W. *Atoms in Molecules: A Quantum Theory*; Oxford University Press: Oxford, UK, 1990.
60. Keith, T.A. TK Gristmill Software. *AIMAll (Version 19.10.12)*, Overland Park, KS, USA, 2019.
61. Morris, G.M.; Huey, R.; Lindstrom, W.; Sanner, M.F.; Belew, R.K.; Goodsell, D.S.; Olson, A.J. AutoDock4 and AutoDockTools4: Automated docking with selective receptor flexibility. *J. Comput. Chem.* **2009**, *30*, 2785–2791. [CrossRef]
62. Valdés-Tresanco, M.S.; Valdés-Tresanco, M.E.; Valiente, P.A.; Moreno, E. AMDock: A versatile graphical tool for assisting molecular docking with Autodock Vina and Autodock4. *Biol. Direct* **2020**, *15*, 12. [CrossRef]
63. Petitpas, I.; Bhattacharya, A.A.; Twine, S.; East, M.; Curry, S. Crystal structure analysis of warfarin binding to human serum albumin. Anatomy of drug site I. *J. Biol. Chem.* **2001**, *276*, 22804–22809. [CrossRef]
64. Drewt, H.R.; Wingtt, R.M.; Takanot, T.; Brokat, C.; Tanakat, S.; Itakuraii, K.; Dickersont, R.E. Structure of a B-DNA dodecamer: Conformation and dynamics. *Proc. Natl. Acad. Sci. USA* **1981**, *78*, 2179–2183.